Visualizing Thermally Activated Conical Intersections Governing Non-Radiative Triplet Decay in a Ni(II) Porphyrin-Nanographene Conjugate with Variable Temperature Transient Absorption Spectroscopy

Saül Garcia-Orrit, Víctor Vega-Mayoral, Qiang Chen, Gianluca Serra, Michele Guizzardi, Valentino Romano, Stefano Dal Conte, Giulio Cerullo, Lorenzo Di Mario, Mordechai Kot, Maria Antonietta Loi, Akimitsu Narita, Klaus Müllen, Matteo Tommasini, and Juan Cabanillas-González*

Visualizing Thermally Activated Conical Intersections Governing Non-Radiative Triplet Decay in a Ni(II) Porphyrin-Nanographene Conjugate with Variable Temperature Transient Absorption Spectroscopy

Saül Garcia-Orrit,[a] Víctor Vega-Mayoral,[a] Qiang Chen,[b] Gianluca Serra,[c] Michele Guizzardi,[d] Valentino Romano,[d] Stefano Dal Conte,[d] Giulio Cerullo,[d] Lorenzo Di Mario,[e] Mordechai Kot,[e] Maria Antonietta Loi,[e] Akimitsu Narita,[b,f] Klaus Müllen,[b,g] Matteo Tommasini,[c] Juan Cabanillas-González,[a]*

[a] Madrid Institute for Advanced Studies, IMDEA Nanociencia, c/Faraday 9, Campus de Cantoblanco, Madrid 28049, Spain.

[b] Max Planck Institute for Polymer Research, Ackermannweg 10, 55128 Mainz, Germany

[c] Dipartimento di Chimica, Materiali ed Ingegneria Chimica "G.Natta", Politecnico di Milano, Piazza Leonardo da Vinci 32, 20133 Milano (Italy)

[d] Dipartimento di Fisica, Politecnico di Milano, Piazza Leonardo Da Vinci, 32, 20133 Milano, Italy

[e] Photophysics and OptoElectronics, Zernike Institute for Advanced Materials, University of Groningen, Nijenborgh 3, 9747 AG, Groningen, The Netherlands

[f] Organic and Carbon Nanomaterials Unit, Okinawa Institute of Science and Technology Graduate University, Okinawa 904-0495, Japan

[g] Institute for Physical Chemistry, Johannes Gutenberg University Mainz, Duesbergweg 10-14, 55128 Mainz, Germany

KEYWORDS: Nanographene, panchromatic, infra-red, photoluminescence, stimulated emission, organic solar cells, metallorganic molecules, infrared sensor.

ABSTRACT: Metalloporphyrins based on open-shell transition metals, such as Ni(II), exhibit typically fast excited-state relaxation. In this work, we shed light into the non-radiative relaxation mechanism in a nanographene - Ni(II) porphyrin conjugate. Variable temperature transient absorption and global fit analysis are combined to produce a picture of the relaxation pathways. At room temperature, photoexcitation of the lowest π–π^* transition is followed by vibrational cooling in 1.6 ps, setting a short 20-ps temporal window wherein a small fraction of relaxed singlets radiatively decay to the ground state before intersystem crossing proceeds. Following intersystem crossing, triplets relax rapidly to the ground state (S_0) in a few tens of picoseconds. By performing measurements at low temperature, we provide evidence for a competition between two terminal relaxation pathways from the lowest (metal-centered) triplet to the ground state: a slow ground state relaxation process proceeding in timescales beyond 1.6 ns and a faster pathway dictated by a sloped conical intersection, which is thermally accessible at room temperature from the triplet state. The overall triplet decay at a given temperature is dictated by the interplay of these two contributions. This observation bears significance in understanding the underlying fast relaxation processes in Ni-based molecules and related transition metal complexes, opening avenues for potential applications for energy harvesting and optoelectronics.

In recent years, transition metal complexes (TMCs) have been the subject of widespread attention for light-to-energy conversion applications like photovoltaics and photocatalysis. [1–7] Focusing on dye-sensitized solar cells (DSSCs), for instance, some TMCs exhibit outstanding performance, acting sequentially as light-harvesting centers and electron donors at the interface with large band gap semiconductor oxides. [8–12] This is, for instance, the case of d^6 octahedral complexes, like $[Ru(bpy)^3]^{2+}$, which is an archetypical light-harvesting antenna in DSSCs. [13–15] The assets of these TMCs stem from

the metal-to-ligand charge transfer (MLCT) character of their lowest triplet states, which are typically long-lived (> 1 μs) and allow for efficient electron transfer before ground state relaxation. [16] These long relaxation timescales are of benefit not only for solar cells but also for photocatalytic applications. [17–19] Despite these notable properties, there is a growing interest in replacing d^6 elements like Ru or Ir with more abundant first-row transition metals.[20]

In other TMCs, like d^8 open-shell Ni complexes, low-lying metal-centered triplet states T(d,d) play a dominant role in the photophysics. In these systems, the T(d,d) states in Ni engage in σ*-antibonding orbitals with the ligands, leading to structural distortion and weakening of the coordination bond, offering a doorway for photoredox reactions. [21,22] It has been confirmed experimentally for instance that the T(d,d) states in Ni(II) aryl halide complexes are responsible for homolysis of the Ni-aryl bond to yield aryl radicals and Ni(I), capable of triggering subsequent catalytical processes. [23] Despite these potentially interesting properties, T(d,d) states undergo a fast non-radiative deactivation, ascribed to a crossing of the triplet and ground state potential energy surfaces (PES), [21–24] thus hindering efficient engagement of Ni-based TMCs with substrates or catalysts by energy or charge transfer. Indeed, sub-nanosecond electronic relaxation is a common observation in many Ni based TMCs, including Ni-pthalocyanines and Ni-porphyrins. [25–28]

Ni-porphyrins have been the subject of investigation with femtosecond optical transient absorption spectroscopy (TAS), X-ray transient absorption spectroscopy and quantum chemical calculations in order to elucidate possible ways to harness energy deactivation. [29,30] This combination of techniques provided insights into the ultrafast electronic and structural relaxation processes of Ni(II) tetramesitylporphyrin (NiTMP), revealing a 1 ps intersystem crossing concomitant with a transition from a ruffled to a planarized porphyrin geometry. [25,30–32] Furthermore, the presence of intermediate triplet states with Ni(I) charge transfer character was unveiled, followed by relaxation towards a triplet T(d,d) state in a few picoseconds. Since Ni(I) can thermally catalyze reactions, these findings offer tantalizing prospects for efficient Ni-photocatalysts, either by the engagement of intermediate states or by changing the nature of the lowest excited triplet state via chemical functionalization. [33] In a recent study, some of us reported on how the fusion of a 5,15-(dimesityl)porphyrin nickel(II) (NiDMP) with two hexa-*peri*-hexabenzocoronenes having two extra K-regions in a symmetric fashion enabled to change the triplet level energetic ordering. [34,35] In this case the large aromatic conjugation pushed the second lowest triplet energy level, of stronger ligand character, below the metal-centered T(d,d) state, which was in turn weakly affected by the conjugation extension. The observed relaxation lifetime from the lowest triplet state was nevertheless only 100 ps and no luminesence was observed.

Hereby, we investigate the ultrafast relaxation processes of a hexa-*peri*-hexabenzocoronene - Ni(II) porphyrin analogue fused in an asymmetric fashion which exhibits unexpected luminescence in the NIR. We combine time-dependent density functional theory (TDDFT) and femtosecond TAS to unravel the electronic relaxation pathways and associated rates as well as the nature of the relevant excited states. Variable temperature TAS (VTTAS) down to 77 K was deployed in a further attempt to elucidate the possible presence of ultrafast thermally activated processes on the photophysics. Our results are compatible with a fast thermally activated access from the triplet to the ground state through a conical intersection between their respective PESs. Detailed analysis of the TAS data provides us with values for the energy barrier and relevant timescales of the thermally activated process, standing as the first experimental observation of this kind in Ni(II) TMCs.

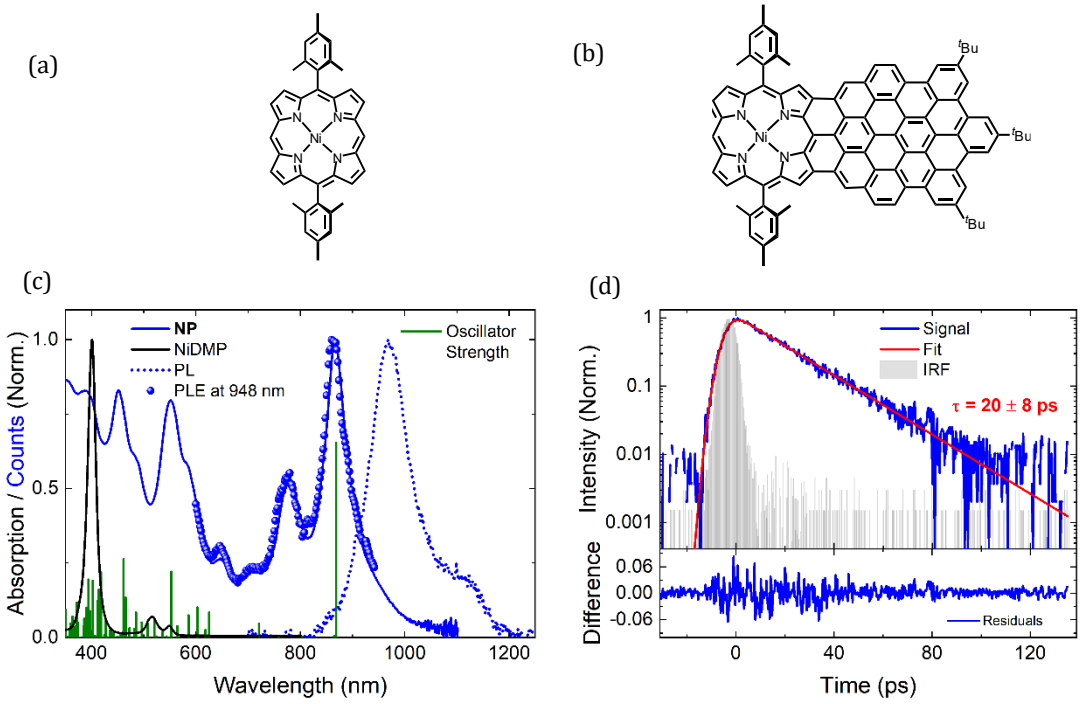

Figure 1. (a-b) Chemical structures of **NiDMP** and **NP,** respectively. (c) Normalized absorption of **NiDMP** and **NP** (black and blue solid lines, respectively) and **NP** PLE (blue dots) and PL (blue dotted line). The green vertical segments indicate the position of optical transitions computed by TDDFT, and their heights are proportional to their oscillator strengths. Excitation (emission) wavelengths employed for PL (PLE) were 780 (948) nm. (d) Room temperature PL dynamics of **NP** detected at 948 nm (blue line) together with a single exponential fit (red line) and instrumental response function (grey shaded area). Residuals from the fit are shown at the bottom (blue line).

Figure 1(a-b) depicts respectively the chemical structure of 5,15-(dimesityl)porphyrin nickel(II) (**NiDMP**) and the compound under study: a NiDMP triply-fused with a π-extended hexa-*peri*-hexabenzocoronene with two K-regions, (hereafter referred as **NP**). Figure 1(c) displays the absorption, photoluminescence excitation (PLE) and emission (PL) spectra of **NP** in methyl-tetrahydrofuran (m-THF). The concentrations of NiDMP and NP in m-THF solution were 43 and 4 μM, respectively. Note that whereas the **NiDMP** absorption is composed by a narrow Soret band at 400 nm and Q bands at 512 nm and 548 nm, the **NP** absorption encompasses wavelengths spanning from the visible to a portion of the near infrared (NIR) spectrum. This phenomenon underscores the significant π-delocalization induced by the fusion of the two planar moieties and highlights the potential of **NP** as an efficient sunlight absorber for solar energy conversion. We performed TDDFT calculations on the **NP** molecule to get information on the electronic states (details are in the ESI). The absorption spectrum computed with TDDFT nicely compares with the experimental one (oscillator strengths are presented in Figure 1(c), more detailed information is exposed in the ESI). The intense band measured at 866 nm / 1.43 eV, and reproduced in the simulated spectrum at 868 nm, is assigned to a transition with large HOMO → LUMO character, corresponding to the lowest bright singlet excited state of **NP** (hereafter referred as $S_1(d_\pi,d_\pi)$). Noteworthy, in contrast to the non-emissive character of **NiDMP**, [36–38] **NP** emits in the NIR, having a PL maximum at 970 nm, and a low energy shoulder at 1103 nm. The observed wavelength spacing between these spectral features ($\Delta\lambda$ = 113 nm or 1242 cm^{-1}) agrees with a predominant vibrational coupling with the collective ring-breathing *D* modes of the graphene moiety, responsible for the Raman peaks located in the 1250 cm^{-1} region, (see Figure S1 in ESI).

PLE measurements were carried out detecting at 948 nm, observing an excellent match with the **NP** absorption spectrum which confirms that the emission arises from **NP** (Figure 1(c)). Noteworthy, replacing m-THF by solvents with larger polarity led to modest PL spectral shifts (see Figure S2), implying a lack of charge transfer character of the excited state responsible for emission, in line with TDDFT calculations. The emissive character of **NP** is somehow unusual in Ni(II)-porphyrins. As Allison and Backer reported, Ni(II) assumes a diamagnetic nature in the porphyrin, inducing an out-of-plane distortion in the ground state, with distinct photophysical attributes in comparison to their planar analogues, comprising reduced fluorescence efficiency and short excited state lifetimes. [30,39]. **NP** bears a PL quantum yield (PLQY) of 1.2 × 10^{-3} (Figure S3) and possesses to the best of our knowledge, one of the deepest near infrared emissions reported among nanographenes. [40–47]

NP exhibits a fast PL decay with a weak temperature dependence; PL lifetimes evolve from 20 ps at 298 K to 26 ps at 4.2 K (Figure 1(d), (Figure S4(a)), suggesting that the main mechanism responsible for S_1 population decay is weakly temperature dependent and mostly ascribed to intersystem crossing due to the inclusion of Ni(II) and the heavy atom effect. [30,39,48]

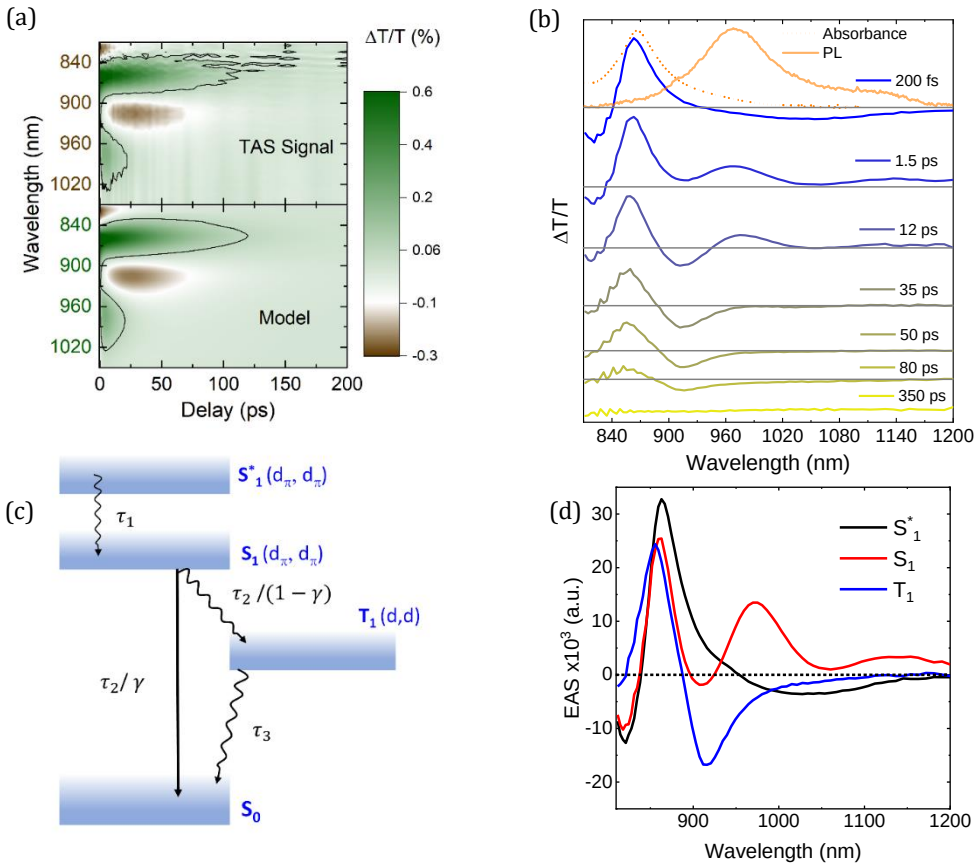

Figure 2. (a) Contour plot of TAS signal (upper plot) and the result reproduced by the model (lower plot) employed to describe the excited state dynamics. ΔT/T = 0 contour lines are depicted as black solid lines. (b) TAS spectra of **NP** at different pump-probe delays. ΔT/T axis is in the same scale for all pump-probe delays, the green arrow represents a 0.8 % ΔT/T signal. (c) Scheme of the photophysical model employed to fit the TAS data. (d) Evolution associated spectra (EAS) of the three excited states involved in the electronic relaxation pathways.

TAS experiments with 120 fs temporal resolution were carried out pumping at 775 nm / 1.60 eV, with 0.3 mJ/cm^2, which led to population of $S_1(d_\pi,d_\pi)$ with an excess of vibrational energy. Note that in the notation employed here, (π,π^*) strictly refers to transitions located in the ligand, whereas (d_π,d_π) denotes transitions involving a mixing of ligand (π) and metal (d) molecular orbitals. No variances in TAS dynamics were observed upon changing the fluence, (Figure S5). The samples were prepared from m-THF based on its glassy transparent nature upon low temperature solidification, which hence allowed to perform low temperature measurements. The TAS contour plot of **NP** at 298 K (Figure 2(a)), depicts positive differential transmission (ΔT/T) values displayed as green shaded areas which stand for ground state bleach (GSB) or stimulated emission (SE), and negative ΔT/T values (brown shaded areas) ascribed to excited state absorption (ESA). Figure 2(b) depicts ΔT/T spectra at fixed delay times corresponding to vertical cuts of the contour plot. The 0.2 ps delay spectrum is dominated by a strong positive peak centered at 863 nm that matches the lowest energy ground state absorption band and is unambiguously assigned to GSB. ESA is observed in the 810-841 nm and 955-1200 nm ranges. At delay times of 1.5 ps two positives ΔT/T bands emerge at 970 nm and 1142 nm emerge, which closely match the PL peaks in Figure 1(c), thus being ascribed to SE. Beyond 4 ps, the GSB and SE spectral bands give way to an oscillatory-like spectrum with positive and negative peaks at 855 and 914 nm, respectively. This oscillatory shape feature dominates the spectrum beyond 35 ps and vanishes in about 135 ps. With the aim of providing a physical interpretation of the TAS data, global fit analysis was applied. The experimental data was successfully reproduced with a photophysical model (Figure 2(c)) involving photoexcitation to populate upper vibrational levels of the lowest singlet excited state (S_1^*), thermalization into S_1 states (τ_1), and subsequent S_1 decay following two branches: ground state decay (τ_2/γ) and intersystem crossing with relaxation in the triplet manifold ($\tau_2/(1-\gamma)$) to yield lowest T_1(d,d) triplet states, (Figure 2(c)). Here, τ_1 stands for the decay time associated to S_1^* thermalization (which encompasses vibrational and solvent relaxation), and τ_2 is the decay time associated to S_1 depopulation; γ stands for the yield of the $S_1 - S_0$ relaxation pathway which we assume it to be negligible compared to the intersystem crossing yield (1-γ), as the γ obtained from the fits are < 0.018 . This assumption is reinforced by the low PLQY (PLQY< 1.2 10^{-3}). TDDFT calculations elucidates the lowest triplet state (T_1(d,d)) located at 0.91 eV above the ground state and described mainly as the HOMO-2 → LUMO+1 transition, which involves two molecular orbitals

localized on the **NP** nickel ion, (Figure S12). The model is completed with fast triplet-to-ground relaxation, mediated via a conical intersection and triplet de-population towards the upper vibrational levels of the ground state (S_0*). Further evidence for this terminal pathway will be provided next with temperature-dependent measurements. In the proposed photophysical model, the T_1-S_0 transition proceeds with a decay time given by τ_3. This model always converges into physical values for the employed parameters and accurately reproduces the TAS matrix, (Figure 2(a) and Figure S6 and S7 in ESI), providing values for the time constants displayed in Table 1. The spectral signatures of each of the three states involved are presented in Figure 2(d).

Noteworthy, the evolution associated spectrum (EAS) of the terminal state possesses an oscillatory shape and its spectral resemblance will be key for the photophysical interpretation in light of temperature-dependent data, displayed and discussed further down. It is important to note that the τ_2 value extracted from the global analysis (16±1 ps) is in line with the S_1 decay time obtained with time-resolved PL measurements (20±8 ps, Figure 1(d)) giving further validity to the excited-state assignments. According to the model, intersystem-crossing proceeds with a time constant of 16 ps, and $T_1 \rightarrow S_0$ proceeds in 40 ps, way faster than the 287 ps lifetime of $T_1 \rightarrow S_0$ transition in the unsubstituted Ni(II) porphyrin. [34] In order to provide further insights on the fast relaxation mechanism involved in the triplet relaxation dynamics, VTTAS measurements at temperatures between 298 K and 77 K were carried out.

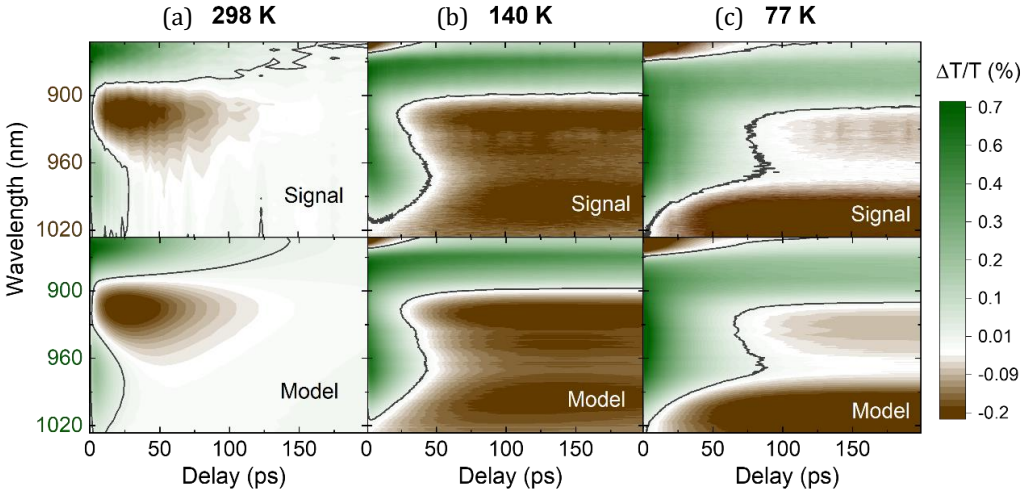

Figure 3. Experimental (top) and reconstructed (bottom) contour TAS plots obtained at (a) 298 K, (b) 140 K and (c) 77 K.

Figure 3(a-c) displays the TAS contour plots at 298K, 140 K and 77 K respectively (the complete set of temperatures is displayed in Figure S7 in ESI). In line with the measurements at 298 K, the low temperature TAS display GSB (centred at 870 nm) and SE (975 nm). It is not surprising that, as temperature is lowered, the GSB and SE signals become more persistent in time in the contour plots. At 140 K, the SE band intensifies and experiences a blueshift, leading to a partial spectral overlap with the GSB band. Noteworthy, a new ESA in the 900 – 1025 nm emerges and becomes clear at 77 K, showing no recovery along the entire 200 ps time window of the measurement. This thermal evolution was further scrutinized in light of the photophysical model shown in Figure 2(c). Interestingly, the TAS spectra and dynamics were perfectly reproduced, as confirmed by the agreement between the experimental and fitted contour plots at 140 K and 77 K (Figure 3(b,c) and Figure S6), and at the rest of the intermediate temperatures (Figure S7). A glance to the EAS obtained at 298 K (Figure 2(d)), 140 K and 77 K (Figure 4a) confirm that the spectra ascribed to S^*_1 and S_1 are comparatively similar, being composed of GSB and ESA (S^*_1) and GSB and SE (S_1). Contrarily, the EAS of the third (T_1) terminal state changes profoundly as the temperature drops, evolving from a first derivative-like feature at 298 K to a spectrum composed of GSB and two broad ESA bands centred at 940 and 1005 nm (EAS evolutions for the entire temperature range are depicted in Figure S8). The associated decay times (τ_1, τ_2 and τ_3) at different temperatures are shown in Figure 4(c,d). Thermalization of S^*_1 gradually slows down as the temperature drops from 298 K to 160 K, probably due to changes in solvent organization and viscosity and their effect on solvent relaxation. Below 160 K, m-THF approaches the glass transition temperature becoming solid, so that the subsequent τ_1 temperature dependence is solely assigned to the effect of temperature on vibrational relaxation. In parallel, with decreasing temperature, S_1 experiences a moderate lifetime increase (τ_2). This could be due to a modest barrier to reach the minimum-energy crossing point between the S_1 and T_1 PESs and/or a slight reduction in the $S_1 - S_0$ non-radiative decay rate. This is consistent with the aforementioned increase in PL lifetime at 4.2 K with respect to 298 K. Comparatively, as the temperature drops from 298 K to 77 K, τ_3 experiences a dramatic increase from 40 ps to 1.48 ns, whereas its temperature dependence resembles a sigmoidal function characteristic of a Maxwell-Boltzmann distribution (Figure 4(c)). This observation prompted us to consider the interplay of two excited-

states, namely the lowest triplet (T_1) and a vibrationally excited ground state (S_0^*), and a thermally activated population transfer between them enabled by a conical intersection, to explain the dramatic change in the EAS and τ_3 of the terminal state upon cooling. The PES crossing point can be accessed via thermal activation, and under such circumstances, the spectral features and time decay of the terminal state are dictated by those of T_1 and S_0^*, (Figure 4(b)). At 298 K, both T_1 and S_0^* are in thermal equilibrium and thus decay with same time constant since S_0^* is continuously repopulated from T_1. Indeed, the interplay of S_0^* is in line with the first derivative-like shape of the terminal EAS, characteristic of a hot ground state since it recalls a superposition of ESA and GSB spectrally offset by the excess of vibrational energy.

At temperatures approaching 77 K, thermal activation is inhibited, and the terminal EAS and decay time bears dominant contribution from the lowest triplet state. At intermediate and room temperatures though, the population of T_1 and S_0^* are thermally equilibrated, both decaying as a sole state with EAS denoted by statistics of the individual spectral contributions. Generically, assuming two excited states (*I* and an higher energy *II*) in thermal equilibrium, the rate constant for depopulation of the equilibrated system is [49]:

$$k = \frac{k_I + k_{II}\exp(-\Delta E/kT)}{1 + \exp(-\Delta E/kT)}$$

with k_I and k_{II} the rate constants for the individual states, kT the thermal energy, ΔE the energy difference between the states and exp ($-\Delta E/kT$) the Boltzmann population factor. On considering the thermal equilibrium with a triplet state, one must bear in mind also the degeneracy and the triplet sublevels. Given that the zero-field splitting is typically well below kT for the temperature range addressed in this study, [49] we can neglect the energy spacing of the triplet sublevels and consider them to decay as a sole state with an average decay time τ_{T1}. Accordingly, the decay time of the equilibrated system would be given by [49–52]:

$$\tau_3(T) = \frac{3 + \exp(-\Delta E/kT)}{\frac{3}{\tau_{T1}} + \frac{1}{\tau^*_{S0}}\exp(-\Delta E/kT)}$$

where ΔE stands for the energy offset between the minimum of the T_1 potential energy surface and the conical intersection, τ^*_{S0} for the decay time of the hot ground state due to vibrational cooling, τ_{T1} the lowest triplet lifetime and 3 denotes the triplet degeneracy. Noteworthy, the expression above provides a good fit to the temperature dependence of τ_3 and provides values of ΔE = 84 ± 9 meV, τ_{T1} = 1.5 ± 0.1 ns and τ_{S0^*} = 1.1 ± 0.8 ps. Further support for the lifetime values obtained by the fit is found in the literature, as we discuss below.

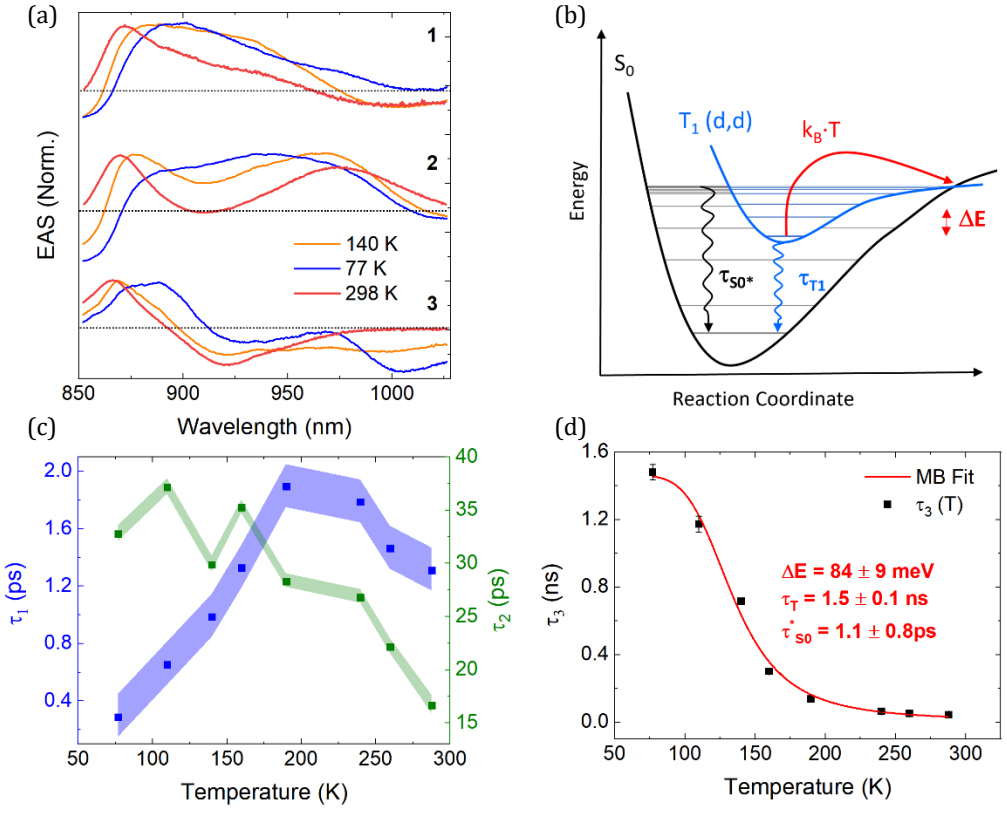

Figure 4. (a) Evolution associated spectra (EAS) of the three excited states at 140 K (depicted in orange) and 77 K (depicted in blue). (b) A schematic representation of the potential energy surfaces, highlighting a thermally activated conical intersection between T_1 and S_0 (in red). (c) Decay times associated to the first two sequential EAS, τ_1 (in blue) and τ_2 (in green), plotted as a function of temperature with the same axis. (d) Decay time of the third EAS (τ_3) as a function of temperature fitted by Eq. 2 (red line). The inset

depicts the activation energy (ΔE) to promote the conical intersection between the lowest triplet (T_1) and the ground state and the respective T_1 and S_0^* lifetimes.

	τ_1 (ps)	τ_2 (ps)	τ_3 (ps)	τ_{PL} (ps)
298 K	1.60 ± 0.15	16.2 ± 0.6	40 ± 0.4	20 ± 8
288 K	1.32 ± 0.15	16.6 ± 0.9	45 ± 0.4	
260 K	1.46 ± 0.15	22.1 ± 0.7	50 ± 0.5	21 ± 8
240 K	1.78 ± 0.15	26.8 ± 0.6	63 ± 0.4	
190 K	1.89 ± 0.15	28.3 ± 0.6	137 ± 0.4	
160 K	1.32 ± 0.15	35.2 ± 0.6	300 ± 0.4	23 ± 8
140 K	0.98 ± 0.15	29.8 ± 0.7	715 ± 0.6	
110 K	0.65 ± 0.15	37.1 ± 0.7	1170 ± 50	25 ± 8
77 K	0.29 ± 0.15	32.7 ± 0.7	1480 ± 50	
60 K				26 ± 8
20 K				26 ± 8
4K				27 ± 8

Table 1. TAS decay time values (τ_1, τ_2, τ_3) and PL decay values measured with a streak camera (τ_{PL}) at different temperatures. The τ_1 error is within our 150 fs temporal resolution.

The obtained value for τ_{S0^*} is therefore assigned to vibrational cooling compatible with similar findings in related molecular systems. Fluorescence up-conversion combined with TAS measurements in free base porphyrins revealed timescales of 100-200 fs for intramolecular vibrational relaxation (IVR) accompanied by a 1.4 ps for vibrational equilibration with the solvent. [53] The presence of a fast subpicosecond IVR component was also confirmed by Abraham in a Zn-TPP with TAS combined with pump-degenerate four-wave mixing. [54] In this case longer 10 and 100 ps decay components were also observed and assigned to vibrational redistribution. More in line with our observations is the work of Eom et al., who unravelled picosecond IVR in Ni(II)TPP and Ni(II)OEP porphyrins. [55] Based on these previous findings the assignment of the picosecond lifetime to vibrational cooling does not seem implausible. The 1.5 ns lifetime found for T_1 is instead tentatively assigned to a T(d,d) state based on the aforementioned TDDFT calculations performed in **NP**. A support for this assignment is the 4 ns decay component reported by Ting et al. and ascribed to the T(d,d) excited state of Ni(II) complex, obtained with 2D nuclear magnetic resonance combined with infrared TAS. [21] The value obtained in our study for the activation energy is roughly three times larger than the available thermal energy at room temperature, evidencing a moderate probability of activation across the barrier compatible with a T_1 PES local minimum located below the conical intersection with S_0.

The picture provided by this study confirms that fast triplet relaxation in Ni-porphyrins could be potentially hindered upon tuning the minimum-energy crossing point between T_1 and S_1. We note that a detailed description of the structural reorganization and the specific reaction coordinates that rule the non-adiabatic crossing of the PESs could provide design strategies addressed to reduce T_1-S_1 thermal activation and harness fast ground state relaxation. Slowing

down T_1(d,d) relaxation in Ni-based TMCs will boost their potential interest for photovoltaics or photocatalysis, where reducing parasitic losses would impact in more efficient light-to-energy conversion. This work highlights the potential of VTTAS combined with global fit analysis to shed light into the nature of non-radiative relaxation processes.

In summary, ultrafast TAS measurements in a panchromatic nanographene-Ni(II) porphyrin conjugate reveal a photophysical scenario comprising fast vibrational relaxation in 1.6 ps and subsequent intersystem crossing in 16 ps, bearing a short temporal window wherein singlets relax to the ground state, as confirmed by a short-lived NIR PL spanning from 850 nm to 1200 nm. Following intersystem crossing, fast relaxation of the triplet to the ground state proceeds in only 40 ps, almost an order of magnitude faster compared to analogous systems. VTTAS combined with global analysis provide further information into this terminal relaxation stage. The results are interpreted in terms of a thermally-induced population transfer from the lowest triplet energy level (a T(d,d) state according to DFT calculations) to a vibrationally excited ground state, enabled through a conical intersection of the respective ground and triplet PESs. The findings presented herein showcase the remarkable potential of VTTAS in deciphering and quantifying rapid thermally activated relaxation phenomena. Such insights hold promise in mitigating intrinsic losses that compete with pivotal photophysical or photochemical reactions crucial for light-to-energy conversion applications.

ASSOCIATED CONTENT

Supporting Information:

- Sample preparation
- TAS experimental details
- PL and TRPL experimental details
- PL and Raman spectra
- PL solvent dependence
- Obtention of **NP** PLQY
- Streak camera measurements at all temperatures
- TAS measurements at all temperatures
- TDDFT quantum chemical calculation details

This material is available free of charge via the Internet at http://pubs.acs.org.

AUTHOR INFORMATION

Corresponding Author

* juan.cabanillas@imdea.org

Author Contributions

The manuscript was written through contributions of all authors. / All authors have given approval to the final version of the manuscript.

Funding Sources

Any funds used to support the research of the manuscript should be placed here (per journal style).

Notes

Any additional relevant notes should be placed here.

ACKNOWLEDGMENT

J.C.-G acknowledges the Spanish Ministry of Science and Innovation (project PID2021-128313OBI00 and reearch consolidation grant CNS2022-136191), the Regional Government of Madrid through projects NMAT2DCM (S2018/NMT-4511), the Proyectos Sinérgicos de I + D (Grant Y2018/NMT-5028 FULMATEN-CM) and NANOCOV-CM (REACT-UE). S.G.-O. is grateful to the Spanish Ministry of Science and Innovation for a Ph.D. grant (FPI, PRE2019-09345). V V.-M. acknowledges grant TED2021-131906A-100 funded by Spanish Ministry of Science, Innovation and Universities (10.13039/501100011033) and support from the Regional Government of Madrid (2019-T2/IND-12737). IMDEA Nanociencia acknowledges support from the Severo Ochoa Programme for Centres of Excellence in R&D (Spanish Ministry of Science and Innovation, grant CEX2020-001039-S). M.T. has been partially supported by ICSC—Centro Nazionale di Ricerca in High-Performance Computing, Big Data, and Quantum Computing funded by the European Union—NextGenerationEU. A.N., and K.M. are grateful for the financial support from the Max Planck Society. Q.C. and A.N. appreciate the financial support from the ANR-DFG NLE Grant GRANAO by DFG 431450789. A.N. is grateful for the financial support from the Okinawa Institute of Science and Technology Graduate University. K.M. acknowledges a fellowship from the Gutenberg Research College, Johannes Gutenberg University Mainz. G.C. and S.D.C. acknowledge financial support by the European Union's Next Generation EU Programme with the IPHOQS Infrastructure (IR0000016, IDD2B8D520, CUP B53C22001750006) "Integrated Infrastructure Initiative in Photonic and Quantum Sciences". M.A.L, L.D.M and M.K. acknowledge the financial support by the European Union (ERC-AdvancedGrant, DEOM, 101 055 097). Views and opinions expressed were however those of the author(s) only and did not necessarily reflect those of the European Union or the European Research Council. Neither the European Union nor the granting authority could be held responsible for them. We would also like to thank Dr. Giuseppe Maria Paternò for helping on the management of this work.

ABBREVIATIONS

NIR (near infrared), NP (hexa-*peri*-hexabenzocoronene-Ni(II) porphyrin), TAS (transient absorption spectroscopy), EAS (evolution associated spectra), TDDFT (time dependent density functional theory), TMP (tetramesitylporphyrin), DMP (dimesitylporphyrin), GSB (ground state bleach), SE (stimulated emission), ESA (excited-state absorption), PES (potential energy surfaces), PL (photoluminescence), PLQY (photoluminescence quantum yield), m-THF (methyl tetrahydrofuran), IVR (intramolecular vibrational relaxation), CI (conical intersection), HOMO (highest occupied molecular orbital), LUMO (lowest unoccupied molecular orbital).

REFERENCES

(1) Gao, Z.; Li, Y.; Xing, J.; Lu, Y.; Shao, Q.; Hu, J.; Zhao, S.; He, W.; Sun, B. Transition Metal Ru(II) Catalysts Immobilized Nanoreactors for Conditional Bioorthogonal Catalysis in Cells. *ACS Appl Mater Interfaces* **2024**, *16* (13), 15870–15878. https://doi.org/10.1021/acsami.3c19133.

(2) Kim, D.; Bhattacharjee, S.; Lam, E.; Casadevall, C.; Rodríguez-Jiménez, S.; Reisner, E. Photocatalytic CO2 Re-

duction Using Homogeneous Carbon Dots with a Molecular Cobalt Catalyst. *Small* **2024**, *2400057*, 1–7. https://doi.org/10.1002/smll.202400057.

(3) Behm, K.; McIntosh, R. D. Application of Discrete First-Row Transition-Metal Complexes as Photosensitisers. *Chempluschem* **2020**, *85* (12), 2611–2618. https://doi.org/10.1002/cplu.202000610.

(4) Dalle, K. E.; Warnan, J.; Leung, J. J.; Reuillard, B.; Karmel, I. S.; Reisner, E. Electro- and Solar-Driven Fuel Synthesis with First Row Transition Metal Complexes. *Chem Rev* **2019**, *119* (4), 2752–2875. https://doi.org/10.1021/acs.chemrev.8b00392.

(5) Wang, P.; Shi, R.; Zhao, J.; Zhang, T. Photodriven Methane Conversion on Transition Metal Oxide Catalyst: Recent Progress and Prospects. *Advanced Science* **2024**, *11* (8), 1–24. https://doi.org/10.1002/advs.202305471.

(6) Matsubara, Y.; Ishitani, O. Photochemical Formation of Hydride Using Transition Metal Complexes and Its Application to Photocatalytic Reduction of the Coenzyme NAD(P)+ and Its Model Compounds. *Coord Chem Rev* **2023**, *477*, 214955. https://doi.org/10.1016/j.ccr.2022.214955.

(7) Kalyanasundaram, K. Applications of Functionalized Transition Metal Complexes in Photonic and Optoelectronic Devices. *Coord Chem Rev* **1998**, *177* (1), 347–414. https://doi.org/10.1016/S0010-8545(98)00189-1.

(8) Polo, A. S.; Itokazu, M. K.; Murakami Iha, N. Y. Metal Complex Sensitizers in Dye-Sensitized Solar Cells. *Coord Chem Rev* **2004**, *248* (13–14), 1343–1361. https://doi.org/10.1016/j.ccr.2004.04.013.

(9) Pashaei, B.; Shahroosvand, H.; Abbasi, P. Transition Metal Complex Redox Shuttles for Dye-Sensitized Solar Cells. *RSC Adv* **2015**, *5* (115), 94814–94848. https://doi.org/10.1039/c5ra13088c.

(10) Chen, C. Y.; Wu, S. J.; Wu, C. G.; Chen, J. G.; Ho, K. C. A Ruthenium Complex with Superhigh Light-Harvesting Capacity for Dye-Sensitized Solar Cells. *Angewandte Chemie - International Edition* **2006**, *45* (35), 5822–5825. https://doi.org/10.1002/anie.200601463.

(11) Sapp, S. A.; Elliott, C. M.; Contado, C.; Caramori, S.; Bignozzi, C. A. Substituted Polypyridine Complexes of Cobalt(II/III) as Efficient Electron-Transfer Mediators in Dye-Sensitized Solar Cells. *J Am Chem Soc* **2002**, *124* (37), 11215–11222. https://doi.org/10.1021/ja027355y.

(12) Bignozzi, C. A.; Argazzi, R.; Boaretto, R.; Busatto, E.; Carli, S.; Ronconi, F.; Caramori, S. The Role of Transition Metal Complexes in Dye Sensitized Solar Devices. *Coord Chem Rev* **2013**, *257* (9–10), 1472–1492. https://doi.org/10.1016/j.ccr.2012.09.008.

(13) Bomben, P. G.; Robson, K. C. D.; Sedach, P. A.; Berlinguette, C. P. On the Viability of Cyclometalated Ru(II) Complexes for Light-Harvesting Applications. *Inorg Chem* **2009**, *48* (20), 9631–9643. https://doi.org/10.1021/ic900653q.

(14) Grätzel, M. Dye-Sensitized Solar Cells. *Journal of Photochemistry and Photobiology C: Photochemistry Reviews* **2003**, *4* (2), 145–153. https://doi.org/10.1016/S1389-5567(03)00026-1.

(15) Clifford, J. N.; Palomares, E.; Md. Nazeeruddin, K.; Grätzel, M.; Durrant, J. R. Dye Dependent Regeneration Dynamics in Dye Sensitized Nanocrystalline Solar Cells: Evidence for the Formation of a Ruthenium Bipyridyl Cation/Iodide Intermediate. *Journal of Physical Chemistry C* **2007**, *111* (17), 6561–6567. https://doi.org/10.1021/jp067458t.

(16) Durrant, J. R.; Haque, S. A.; Palomares, E. Towards Optimisation of Electron Transfer Processes in Dye Sensitised Solar Cells. *Coord Chem Rev* **2004**, *248* (13–14), 1247–1257. https://doi.org/10.1016/j.ccr.2004.03.014.

(17) Teplý, F. Visible-Light Photoredox Catalysis with [Ru(Bpy)3]2+: General Principles and the Twentieth-Century Roots. *Physical Sciences Reviews* **2020**, *5* (4), 1–19. https://doi.org/10.1515/psr-2017-0171.

(18) Koike, T.; Akita, M. Visible-Light Radical Reaction Designed by Ru- and Ir-Based Photoredox Catalysis. *Inorg Chem Front* **2014**, *1* (8), 562–576. https://doi.org/10.1039/c4qi00053f.

(19) White, T. A.; Higgins, S. L. H.; Arachchige, S. M.; Brewer, K. J. Efficient Photocatalytic Hydrogen Production in a Single-Component System Using Ru,Rh,Ru Supramolecules Containing 4,7-Diphenyl-1,10-Phenanthroline. *Angewandte Chemie - International Edition* **2011**, *50* (51), 12209–12213. https://doi.org/10.1002/anie.201105170.

(20) Bozic-Weber, B.; Constable, E. C.; Housecroft, C. E. Light Harvesting with Earth Abundant D-Block Metals: Development of Sensitizers in Dye-Sensitized Solar Cells (DSCs). *Coord Chem Rev* **2013**, *257* (21–22), 3089–3106. https://doi.org/10.1016/j.ccr.2013.05.019.

(21) Ting, S. I.; Garakyaraghi, S.; Taliaferro, C. M.; Shields, B. J.; Scholes, G. D.; Castellano, F. N.; Doyle, A. G. 3d-d Excited States of Ni(II) Complexes Relevant to Photoredox Catalysis: Spectroscopic Identification and Mechanistic Implications. *ACS Appl Mater Interfaces* **2020**, 142, 5800-5810. https://doi.org/10.1021/jacs.0c00781.

(22) Ogawa, T.; Sinha, N.; Pfund, B.; Prescimone, A.; Wenger, O. S. Molecular Design Principles to Elongate the Metal-to-Ligand Charge Transfer Excited-State Lifetimes of Square-Planar Nickel(II) Complexes. *J Am Chem Soc* **2022**, *144* (48), 21948–21960. https://doi.org/10.1021/jacs.2c08838.

(23) Wegeberg, C.; Wenger, O. S. Luminescent First-Row Transition Metal Complexes. *JACS Au* **2021**, *1* (11), 1860–1876. https://doi.org/10.1021/jacsau.1c00353.

(24) Hou, C. L.; Song, J. X.; Chang, X.; Chen, Y. Photoluminescent Nickel(II) Carbene Complexes with Ligand-to-Ligand Charge-Transfer Excited States. *Chinese Chemical Letters* **2024**, *35* (1), 108333. https://doi.org/10.1016/j.cclet.2023.108333.

(25) Zhang, X.; Wasinger, E. C.; Muresan, A. Z.; Attenkofer, K.; Jennings, G.; Lindsey, J. S.; Chen, L. X. Ultrafast Stimulated Emission and Structural Dynamics in Nickel Porphyrins. *Journal of Physical Chemistry A* **2007**, *111* (46), 11736–11742. https://doi.org/10.1021/jp0751763.

(26) Xiao, Z.; Li, Z.; Wu, X.; Fang, Y.; Ao, G.; Huang, J.; Liu, D.; Wang, Y.; Zhang, X.; Song, Y. Ultrafast Excited-State Dy-

namics of Ni-Contained Covalently Bonded Phthalocyanine-Porphyrin Conjugates. *Dyes and Pigments* **2016**, *127*, 197–203. https://doi.org/10.1016/j.dyepig.2015.10.026.

(27) Rodriguez, J.; Holten, D. Ultrafast Vibrational Dynamics of a Photoexcited Metalloporphyrin. *J Chem Phys* **1989**, *91* (6), 3525–3531. https://doi.org/10.1063/1.456883.

(28) Naumova, M. A.; Paveliuc, G.; Biednov, M.; Kubicek, K.; Kalinko, A.; Meng, J.; Liang, M.; Rahaman, A.; Abdellah, M.; Checchia, S.; Alves Lima, F.; Zalden, P.; Gawelda, W.; Bressler, C.; Geng, H.; Lin, W.; Liu, Y.; Zhao, Q.; Pan, Q.; Akter, M.; Kong, Q.; Retegan, M.; Gosztola, D. J.; Pápai, M.; Khakhulin, D.; Lawson Daku, M.; Zheng, K.; Canton, S. E. Nonadiabatic Charge Transfer within Photoexcited Nickel Porphyrins. *Journal of Physical Chemistry Letters* **2024**, *15* (13), 3627–3638. https://doi.org/10.1021/acs.jpclett.4c00375.

(29) Phelan, B. T.; Mara, M. W.; Chen, L. X. Excited-State Structural Dynamics of Nickel Complexes Probed by Optical and X-Ray Transient Absorption Spectroscopies: Insights and Implications. *Chemical Communications* **2021**, *57* (90), 11904–11921. https://doi.org/10.1039/d1cc03875c.

(30) Shelby, M. L.; Lestrange, P. J.; Jackson, N. E.; Haldrup, K.; Mara, M. W.; Stickrath, A. B.; Zhu, D.; Lemke, H. T.; Chollet, M.; Hoffman, B. M.; Li, X.; Chen, L. X. Ultrafast Excited State Relaxation of a Metalloporphyrin Revealed by Femtosecond X-Ray Absorption Spectroscopy. *J Am Chem Soc* **2016**, *138* (28), 8752–8764. https://doi.org/10.1021/jacs.6b02176.

(31) Chen, L. X.; Zhang, X.; Wasinger, E. C.; Attenkofer, K.; Jennings, G.; Muresan, A. Z.; Lindsey, J. S. Tracking Electrons and Atoms in a Photoexcited Metalloporphyrin by X-Ray Transient Absorption Spectroscopy. *J Am Chem Soc* **2007**, *129* (31), 9616–9618. https://doi.org/10.1021/ja072979v.

(32) Zamyatin, A. V.; Soldatova, A. V.; Rodgers, M. A. J. The Photophysics of Ni(II) Meso-Tetraphenylbenzoporphyrin: A Combined Theoretical and Experimental Investigation. *Inorganica Chim Acta* **2007**, *360* (3), 857–868. https://doi.org/10.1016/j.ica.2006.06.031.

(33) Wong, Y. S.; Tang, M. C.; Ng, M.; Yam, V. W. W. Toward the Design of Phosphorescent Emitters of Cyclometalated Earth-Abundant Nickel(II) and Their Supramolecular Study. *J Am Chem Soc* **2020**, *142* (16), 7638–7646. https://doi.org/10.1021/jacs.0c02172.

(34) Garcia-Orrit, S.; Vega-Mayoral, V.; Chen, Q.; Serra, G.; Paternò, G. M.; Cánovas, E.; Narita, A.; Müllen, K.; Tommasini, M.; Cabanillas-González, J. Nanographene-Based Decoration as a Panchromatic Antenna for Metalloporphyrin Conjugates. *Small* **2023**, *19* (42), 1–7. https://doi.org/10.1002/smll.202301596.

(35) Chen, Q.; Brambilla, L.; Daukiya, L.; Mali, K. S.; De Feyter, S.; Tommasini, M.; Müllen, K.; Narita, A. Synthesis of Triply Fused Porphyrin-Nanographene Conjugates. *Angewandte Chemie - International Edition* **2018**, *57* (35), 11233–11237. https://doi.org/10.1002/anie.201805063.

(36) Wolf, M.; Lungerich, D.; Bauroth, S.; Popp, M.; Platzer, B.; Clark, T.; Anderson, H. L.; Jux, N.; Guldi, D. M. Panchromatic Light Funneling through the Synergy in Hexabenzocoronene-(Metallo)Porphyrin-Fullerene Assemblies to Realize the Separation of Charges. *Chem Sci* **2020**, *11* (27), 7123–7132. https://doi.org/10.1039/d0sc02028a.

(37) Wang, W. C.; Lin, Y. W.; Peng, S. H.; Chuang, C. T.; Chang, C. C.; Hsu, C. S. A Strategy of Designing Near-Infrared Porphyrin-Based Non-Fullerene Acceptors for Panchromatic Organic Solar Cells. *Org Electron* **2020**, *86* (June), 105899. https://doi.org/10.1016/j.orgel.2020.105899.

(38) Shiu, J. W.; Chang, Y. C.; Chan, C. Y.; Wu, H. P.; Hsu, H. Y.; Wang, C. L.; Lin, C. Y.; Diau, E. W. G. Panchromatic Co-Sensitization of Porphyrin-Sensitized Solar Cells to Harvest near-Infrared Light beyond 900 Nm. *J Mater Chem A Mater* **2015**, *3* (4), 1417–1420. https://doi.org/10.1039/c4ta06589a.

(39) Allison, J. B.; Becker, R. S. Effect of Metal Atom Perturbations on the Luminescent Spectra of Porphyrins. *J Chem Phys* **1960**, *32* (5), 1410–1417. https://doi.org/10.1063/1.1730932.

(40) Mahlmeister, B.; Mahl, M.; Reichelt, H.; Shoyama, K.; Stolte, M.; Würthner, F. Helically Twisted Nanoribbons Based on Emissive Near-Infrared Responsive Quaterrylene Bisimides. *J Am Chem Soc* **2022**, *144* (23), 10507–10514. https://doi.org/10.1021/jacs.2c02947.

(41) Xu, X.; Muñoz-Mármol, R.; Vasylevskyi, S.; Villa, A.; Folpini, G.; Scotognella, F.; Maria Paternò, G.; Narita, A. Synthesis of Bioctacene-Incorporated Nanographene with Near-Infrared Chiroptical Properties. *Angewandte Chemie - International Edition* **2023**, *62* (14), 1–5. https://doi.org/10.1002/anie.202218350.

(42) Muñoz-Mármol, R.; Gordillo, F.; Bonal, V.; Villalvilla, J. M.; Boj, P. G.; Quintana, J. A.; Ross, A. M.; Paternò, G. M.; Scotognella, F.; Lanzani, G.; Derradji, A.; Sancho-García, J. C.; Gu, Y.; Wu, J.; Casado, J.; Díaz-García, M. A. Near-Infrared Lasing in Four-Zigzag Edged Nanographenes by 1D versus 2D Electronic π-Conjugation. *Adv Funct Mater* **2021**, *31*, (41), 2105073. https://doi.org/10.1002/adfm.202105073.

(43) Paternò, G. M.; Chen, Q.; Munõz-Mármol, R.; Guizzardi, M.; Bonal, V.; Kabe, R.; Barker, A. J.; Boj, P. G.; Chatterjee, S.; Ie, Y.; Villalvilla, J. M.; Quintana, J. A.; Scotognella, F.; Müllen, K.; Diáz-Garciá, M. A.; Narita, A.; Lanzani, G. Excited States Engineering Enables Efficient Near-Infrared Lasing in Nanographenes. *Mater Horiz* **2022**, *9* (1), 393–402. https://doi.org/10.1039/d1mh00846c.

(44) Gu, Y.; Vega-Mayoral, V.; Garcia-Orrit, S.; Schollmeyer, D.; Narita, A.; Cabanillas-González, J.; Qiu, Z.; Müllen, K. Cove-Edged Hexa-Peri-Hexabenzo-Bis-Peri-Octacene: Molecular Conformations and Amplified Spontaneous Emission. *Angewandte Chemie - International Edition* **2022**, *61*, (18), e202201088. https://doi.org/10.1002/anie.202201088.

(45) Pun, S. H.; Cheung, K. M.; Yang, D.; Chen, H.; Wang, Y.; Kershaw, S. V.; Miao, Q. A Near-Infrared Absorbing and Emissive Quadruple Helicene Enabled by the Scholl Reaction of Perylene. *Angewandte Chemie - International Edition* **2022**, *61*, (8), e202113203. https://doi.org/10.1002/anie.202113203.

(46) He, H.; Lee, Y. J.; Zong, Z.; Liu, N.; Lynch, V. M.; Kim, J.; Oh, J.; Kim, D.; Sessler, J. L.; Ke, X. S. Nanographene-Fused Expanded Carbaporphyrin Tweezers. *J Am Chem Soc* **2024**, *146* (1), 543–551. https://doi.org/10.1021/jacs.3c10122.

(47) Tan, J.; Xu, X.; Liu, J.; Vasylevskyi, S.; Lin, Z.; Kabe, R.; Zou, Y.; Müllen, K.; Narita, A.; Hu, Y. Synthesis of a π-Extended Double [9]Helicene. *Angewandte Chemie - International Edition* **2023**, *62*, (18), e202218494. https://doi.org/10.1002/anie.202218494.

(48) Habib, A.; Serniabad, S.; Khan, M. S.; Islam, R.; Chakraborty, M.; Nargis, A.; Quayum, M. E.; Alam, M. A.; rapozzi, V.; Tabata, M. Kinetics and Mechanism of Formation of Nickel(II)Porphyrin and Its Interaction with DNA in Aqueous Medium. *Journal of Chemical Sciences* **2021**, *133,* (3), 83. https://doi.org/10.1007/s12039-021-01945-y.

(49) Striplin, D. R.; Crosby, G. A. Nature of the Emitting 3MLCT Manifold of Rhenium(I) (Diimine) (CO) 3Cl Complexes. *Chem Phys Lett* **1994**, *221* (5–6), 426–430. https://doi.org/10.1016/0009-2614(94)00282-7.

(50) Hofbeck, T.; Monkowius, U.; Yersin, H. Highly Efficient Luminescence of Cu(I) Compounds: Thermally Activated Delayed Fluorescence Combined with Short-Lived Phosphorescence. *J Am Chem Soc* **2015**, *137* (1), 399–404. https://doi.org/10.1021/ja5109672.

(51) Leitl, M. J.; Küchle, F. R.; Mayer, H. A.; Wesemann, L.; Yersin, H. Brightly Blue and Green Emitting Cu(I) Dimers for Singlet Harvesting in OLEDs. *Journal of Physical Chemistry A* **2013**, *117* (46), 11823–11836. https://doi.org/10.1021/jp402975d.

(52) Sun, C.; Llanos, L.; Arce, P.; Oliver, A.; Wannemacher, R.; Cabanillas-Gonzalez, J.; Lemus, L.; Aravena, D. Nuclearity Control for Efficient Thermally Activated Delayed Fluorescence in a CuI Complex and Its Halogen-Bridged Dimer. *Chemistry of Materials* **2021**, *33* (16), 6383–6393. https://doi.org/10.1021/acs.chemmater.1c01531.

(53) Baskin, J. S.; Yu, H. Z.; Zewail, A. H. Ultrafast Dynamics of Porphyrins in the Condensed Phase: I. Free Base Tetraphenylporphyrin. *Journal of Physical Chemistry A* **2002**, *106* (42), 9837–9844. https://doi.org/10.1021/jp020398g.

(54) Abraham, B.; Nieto-Pescador, J.; Gundlach, L. Ultrafast Relaxation Dynamics of Photoexcited Zinc-Porphyrin: Electronic-Vibrational Coupling. *Journal of Physical Chemistry Letters* **2016**, *7* (16), 3151–3156. https://doi.org/10.1021/acs.jpclett.6b01439.

(55) Eom, H. S.; Jeoung, S. C.; Kim, D.; Ha, J.-H.; Kim, Y.-R. Ultrafast Vibrational Relaxation and Ligand Photodissociation/Photoassociation Processes of Nickel(II) Porphyrins in the Condensed Phase. *J Phys Chem A* **1997**, *101* (20), 3661–3669. https://doi.org/10.1021/jp962374d.

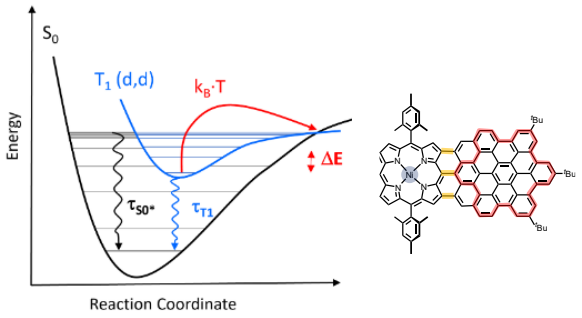

Table of Contents artwork